



Manufacturing with light - micro-assembly of opto-electronic microstructures

SHUAILONG ZHANG,^{1,2,9} YONGPENG LIU,^{1,3} YANG QIAN,¹ WEIZHEN LI,¹ JOAN JUVERT,^{4,5} PENGFEI TIAN,⁶ JEAN-CLAUDE NAVARRO,⁷ ALASDAIR W CLARK,¹ ERDAN GU,⁸ MARTIN D. DAWSON,⁸ JONATHAN M. COOPER,¹ AND STEVEN L. NEALE^{1,10}

¹*School of Engineering, University of Glasgow, Glasgow, Scotland, G12 8LT, UK*

²*Current address: Department of Chemistry, University of Toronto, Toronto, Ontario, M5S 3H6, Canada*

³*Current address: Laboratory for Molecular Engineering of Optoelectronic Nanomaterials, Institute of Chemical Sciences and Engineering, École Polytechnique Fédérale de Lausanne, CH-1015 Lausanne, Switzerland*

⁴*Photonics Research Group, INTEC, Ghent University-IMEC, iGent Tower, 9052 Ghent, Belgium*

⁵*Center for Nano- and Biophotonics, Ghent University, iGent Tower, 9052 Ghent, Belgium*

⁶*Institute for Electric Light Sources, Fudan University, Shanghai, 200433, China*

⁷*IPS, 24A, rue de la Résistance, BP 438, 74108 ANNEMASSE Cedex, France*

⁸*Institute of Photonics, Department of Physics, University of Strathclyde, Glasgow, Scotland, G1 1RD, UK*

⁹*shuailong.zhang@utoronto.ca*

¹⁰*steven.neale@glasgow.ac.uk*

Abstract: Optical micromanipulation allows the movement and patterning of discrete micro-particles within a liquid environment. However, for manufacturing applications it is desirable to remove the liquid, leaving the patterned particles in place. In this work, we have demonstrated the use of optoelectronic tweezers (OET) to manipulate and accurately assemble Sn₆₂Pb₃₆Ag₂ solder microspheres into tailored patterns. A technique based on freeze-drying technology was then developed that allows the assembled patterns to be well preserved and fixed in place after the liquid medium in the OET device is removed. After removing the liquid from the OET device and subsequently heating the assembled pattern and melting the solder microspheres, electrical connections between the microspheres were formed, creating a permanent conductive bridge between two isolated metal electrodes. Although this method is demonstrated with 40 μm diameter solder beads arranged with OET, it could be applied to a great range of discrete components from nanowires to optoelectronic devices, thus overcoming one of the basic hurdles in using optical micromanipulation techniques in a manufacturing micro-assembly setting.

Published by The Optical Society under the terms of the [Creative Commons Attribution 4.0 License](#). Further distribution of this work must maintain attribution to the author(s) and the published article's title, journal citation, and DOI.

OCIS codes: (350.4855) Optical tweezers or optical manipulation; (120.4610) Optical fabrication; (120.4880) Optomechanics.

References and links

1. A. Ashkin, J. M. Dziedzic, and T. Yamane, "Optical trapping and manipulation of single cells using infrared laser beams," *Nature* **330**(6150), 769–771 (1987).
2. D. G. Grier, "A revolution in optical manipulation," *Nature* **424**(6950), 810–816 (2003).
3. L. Paterson, M. MacDonald, J. Arlt, W. Sibbett, P. Bryant, and K. Dholakia, "Controlled rotation of optically trapped microscopic particles," *Science* **292**(5518), 912–914 (2001).
4. M. Zhong, X. Wei, J. Zhou, Z. Wang, and Y. Li, "Trapping red blood cells in living animals using optical tweezers," *Nat. Comm.* **4**, 1768 (2013).
5. X. Ding, Z. Peng, S.-C. S. Lin, M. Geri, S. Li, P. Li, Y. Chen, M. Dao, S. Suresh, and T. J. Huang, "Cell separation using tilted-angle standing surface acoustic waves," *Proc. Natl. Acad. Sci. U.S.A.* **111**(36), 12992–12997 (2014).
6. F. Guo, Z. Mao, Y. Chen, Z. Xie, J. P. Lata, P. Li, L. Ren, J. Liu, J. Yang, M. Dao, S. Sureshd, and T. J. Huang, "Three-dimensional manipulation of single cells using surface acoustic waves," *Proc. Natl. Acad. Sci. U.S.A.* **113**(6), 1522–1527 (2016).

7. R. Pethig, "Dielectrophoresis: Status of the theory, technology, and applications," *Biomicrofluidics* **4**(2), 022811 (2010).
 8. P. Y. Chiou, A. T. Ohta, and M. C. Wu, "Massively parallel manipulation of single cells and microparticles using optical images," *Nature* **436**(7049), 370–372 (2005).
 9. A. T. Ohta, M. Garcia, J. K. Valley, L. Banie, H.-Y. Hsu, A. Jamshidi, S. L. Neale, T. Lue, and M. C. Wu, "Motile and non-motile sperm diagnostic manipulation using optoelectronic tweezers," *Lab Chip* **10**(23), 3213–3217 (2010).
 10. S. M. Yang, T. M. Yu, H. P. Huang, M. Y. Ku, L. Hsu, and C. H. Liu, "Dynamic manipulation and patterning of microparticles and cells by using TiOPc-based optoelectronic dielectrophoresis," *Opt. Lett.* **35**(12), 1959–1961 (2010).
 11. A. Zarowna-Dabrowska, S. L. Neale, D. Massoubre, J. McKendry, B. R. Rae, R. K. Henderson, M. J. Rose, H. Yin, J. M. Cooper, E. Gu, and M. M. Dawson, "Miniaturized optoelectronic tweezers controlled by GaN micro-pixel light emitting diode arrays," *Opt. Exp.* **19**(3), 2720–2728 (2011).
 12. S. L. Neale, A. T. Ohta, H. Y. Hsu, J. K. Valley, A. Jamshidi, and M. C. Wu, "Trap profiles of projector based optoelectronic tweezers (OET) with HeLa cells," *Opt. Exp.* **17**(7), 5231–5239 (2009).
 13. W. Choi, S. W. Nam, H. Hwang, S. Park, and J. K. Park, "Programmable manipulation of motile cells in optoelectronic tweezers using a grayscale image," *Appl. Phys. Lett.* **93**(14), 143901 (2008).
 14. J. K. Valley, S. Neale, H. Y. Hsu, A. T. Ohta, A. Jamshidi, and M. C. Wu, "Parallel single-cell light-induced electroporation and dielectrophoretic manipulation," *Lab Chip* **9**(12), 1714–1720 (2009).
 15. H. Hwang and J. K. Park, "Optoelectrofluidic platforms for chemistry and biology," *Lab Chip* **11**(1), 33–47 (2011).
 16. M. Woerdemann, C. Alpmann, M. Esseling, and C. Denz, "Advanced optical trapping by complex beam shaping," *Laser Photon. Rev.* **7**(6), 839–854 (2013).
 17. A. Jamshidi, P. J. Pauzauskie, P. J. Schuck, A. T. Ohta, P. Y. Chiou, J. Chou, P. Yang, and M. C. Wu, "Dynamic manipulation and separation of individual semiconducting and metallic nanowires," *Nat. Photon.* **2**(2), 86–89 (2008).
 18. P. J. Pauzauskie, A. Jamshidi, J. K. Valley, J. H. Satcher Jr, and M. C. Wu, "Parallel trapping of multiwalled carbon nanotubes with optoelectronic tweezers," *Appl. Phys. Lett.* **95**(11), 113104 (2009).
 19. A. Jamshidi, S. L. Neale, K. Yu, P. J. Pauzauskie, P. J. Schuck, J. K. Valley, H. Y. Hsu, A. T. Ohta, and M. C. Wu, "Nanopen: Dynamic, Low-power, and Light-actuated Patterning of Nanoparticles," *Nano Lett.* **9**(8), 2921–2925 (2009).
 20. S. Zhang, Y. Liu, J. Juvert, P. Tian, J. C. Navarro, J. M. Cooper, and S. L. Neale, "Use of optoelectronic tweezers in manufacturing - accurate solder bead positioning," *Appl. Phys. Lett.* **109**(22), 221110 (2016).
 21. S. Zhang, J. Juvert, J. M. Cooper, and S. L. Neale, "Manipulating and assembling metallic beads with optoelectronic tweezers," *Sci. Rep.* **6**, 32840 (2016).
 22. J. Juvert, S. Zhang, I. Eddie, C. J. Mitchell, G. T. Reed, J. S. Wilkinson, A. Kelly, and S. L. Neale, "Micromanipulation of InP lasers with optoelectronic tweezers for integration on a photonic platform," *Opt. Exp.* **24**(16), 18163–18175 (2016).
 23. S. C. Chapin, V. Germain, and E. R. Dufresne, "Automated trapping, assembly, and sorting with holographic optical tweezers," *Opt. Exp.* **14**(26), 13095–13100 (2006).
 24. K. D. Hermanson, S. O. Lumsdon, J. P. Williams, E. W. Kaler, and O. D. Velev, "Dielectrophoretic assembly of electrically functional microwires from nanoparticle suspensions," *Science* **294**(5544), 1082–1086 (2001).
 25. R. J. Barsotti, M. D. Vahey, R. Wartena, Y. M. Chiang, J. Voldman, and F. Stellacci, "Assembly of metal nanoparticles into nanogaps," *Small* **3**(3), 488–499 (2007).
 26. M. C. Tien, A. T. Ohta, K. Yu, S. L. Neale, and M. C. Wu, "Heterogeneous integration of InGaAsP microdisk laser on a silicon platform using optofluidic assembly," *Appl. Phys. A* **95**(4), 967–972 (2009).
 27. H. Yang, D. Zhao, S. Chuwongin, J. H. Seo, W. Yang, Y. Shuai, J. Berggren, M. Hammar, Z. Ma, and W. Zhou, "Transfer-printed stacked nanomembrane lasers on silicon," *Nat. Photon.* **6**(9), 615–620 (2012).
 28. B. Guilhabert, A. Hurtado, D. Jevtics, Q. Gao, H. H. Tan, C. Jagadish, and M. D. Dawson, "Transfer printing of semiconductor nanowires with lasing emission for controllable nanophotonic device fabrication," *ACS nano* **10**(4), 3951–3958 (2016).
 29. S. I. Park, Y. Xiong, R. H. Kim, P. Elvikis, M. Meitl, D. H. Kim, J. Wu, J. Yoon, C. J. Yu, Z. Liu, Y. Huang, K. Hwang, P. Ferreira, X. Li, K. Choquette, and J. A. Rogers, "Printed assemblies of inorganic light-emitting diodes for deformable and semitransparent displays," *Science* **325**(5943), 977–981 (2009).
 30. C. J. Kim, J. Y. Kim, and B. Sridharan, "Comparative evaluation of drying techniques for surface micromachining," *Sens. Actuator A* **64**(1), 17–26 (1998).
 31. A. G. Marin, O. R. Enriquez, P. Brunet, P. Colinet, and J. H. Snoeijer, "Universality of tip singularity formation in freezing water drops," *Phys. Rev. Lett.* **113**(5), 054301 (2014).
 32. A. J. Trindade, B. Guilhabert, D. Massoubre, D. Zhu, N. Laurand, E. Gu, I. M. Watson, C. J. Humphreys, and M. D. Dawson, "Nanoscale-accuracy transfer printing of ultra-thin AlInGaN light-emitting diodes onto mechanically flexible substrates," *Appl. Phys. Lett.* **103**(25), 253302 (2013).
 33. A. J. Trindade, B. Guilhabert, E. Y. Xie, R. Ferreira, J. J. D. McKendry, D. Zhu, N. Laurand, E. Gu, D. J. Wallis, I. M. Watson, C. J. Humphreys, and M. D. Dawson, "Heterogeneous integration of Gallium Nitride light-emitting diodes on diamond and silica by transfer printing," *Opt. Exp.* **23**(7), 9329–9338 (2015).
-

1. Introduction

Micromanipulation technologies such as optical tweezers [1–4], acoustic tweezers [5, 6] and dielectrophoresis (DEP) [7] allow the fine and non-invasive control and actuation of discrete micro/nano-scale objects with no physical contact for studies in physics, chemistry and particularly biological and medical science. More recently, optoelectronic tweezers (OET) have been demonstrated as a new opto-electro-fluidic micromanipulation technology using light-patterned DEP for biological applications such as cell sorting, cell patterning and studying cell-to-cell communications [8–15]. Compared to conventional optical tweezers [16], which operate by transferring optical momentum from the light beam to the object, OET traps exert a much stronger manipulation force for a given intensity of light, and are well suited for massively parallel manipulation (e.g. 15,000 traps at once with just 1 mW of optical power) [8, 12]. OET has also been used to assemble nanoscale electronic and photonic components such as semiconductor nanowires, carbon nanotubes and metallic spherical nanocrystals for microfabrication applications [17–19]. Additionally, there is a growing interest in using OET to manipulate and assemble large electronic/photonic components with scales of tens up to several hundreds of microns, such as large metallic beads, standard surface-mount-technology components and semiconductor micro-lasers [20–22].

Previous work has demonstrated the micromanipulation and assembly of many different particle types using several different micromanipulation techniques including the automated assembly of micro-particles with optical tweezers [23] and the assembly of gold nanoparticles with DEP [24, 25]. These studies show that complex patterns of micro and nanoparticles can be created in liquids but the stability of the assembled structures can depend on the particles. Assembly of single cells into desired arrangements using acoustic tweezing has also recently been demonstrated [6]. One example application of this kind of assembly is the construction of a micro-scale circuit containing small electrical components using OET. For this application, it is necessary to first place the component into the desired position and then to fix it into place. Recently, it has been shown that large metallic beads can be positioned using OET with submicron accuracy [20, 21]. However, a major bottleneck of using OET to assemble these beads and construct a microscale circuit is the lack of the ability to fix the assembled beads in place whilst removing the liquid medium. Previously-reported work has demonstrated the use of a photocurable polymer solution to preserve the positions of the nanowires trapped by OET, which is achieved by immobilizing the nanowires by polymerizing the solution [17]. However, the polymer solution was found to reduce the exerted force on the nanowires significantly due to its high viscosity and conductivity. Additionally, after photocuring the polymer solution, it is difficult to perform further processes on the assembled nanowires. Some components can be held in position whilst the liquid is removed [26]. However, it was also found that as the liquid dries out, the components depending on their geometry may be dragged away from the desired position by buffer's meniscus. Therefore, it is desirable to develop a more widely applicable method of fixing the assembled micro-objects in place in a micromanipulation system whilst removing the liquid medium.

In this work, we have demonstrated the use of OET to assemble 40 μm diameter $\text{Sn}_{62}\text{Pb}_{36}\text{Ag}_2$ solder microspheres to form electrical connections with low resistance. After assembling the solder microspheres with OET, we have implemented a new method based on freeze-drying to remove the liquid medium. We freeze the liquid medium in the OET device and then reduce the surrounding pressure to allow the frozen medium to sublime directly from its solid phase to its gas phase. This method allows the assembled solder beads to be well preserved and fixed in place in the OET device after the liquid medium is removed. Based on this method, we demonstrated using OET to construct a microscale circuit with solder microspheres assembled into a straight line to connect two isolated metal contacts with 200 μm gap. After removing the liquid in the OET device with an optimized step-by-step freeze-drying process and subsequently heating the assembled

solder microspheres to melt them together, electrical connections between the isolated metal contacts were formed with resistances as low as 11.6Ω . Scanning electron microscope (SEM) (Hitachi S4700) images were taken at the interfaces between the two metal contacts connected by the solder microspheres, which showed that the surfaces of the microspheres became textured and physical connections between the adjacent microspheres were formed after the heating and melting process. Analysis suggested that the heating process melted the materials at the surface of the solder microspheres and thus enabled to form electrical connections between adjacent microspheres with much reduced interface resistance. By using these combined techniques, micro-electrical connections between the isolated metal contacts have been successfully created.

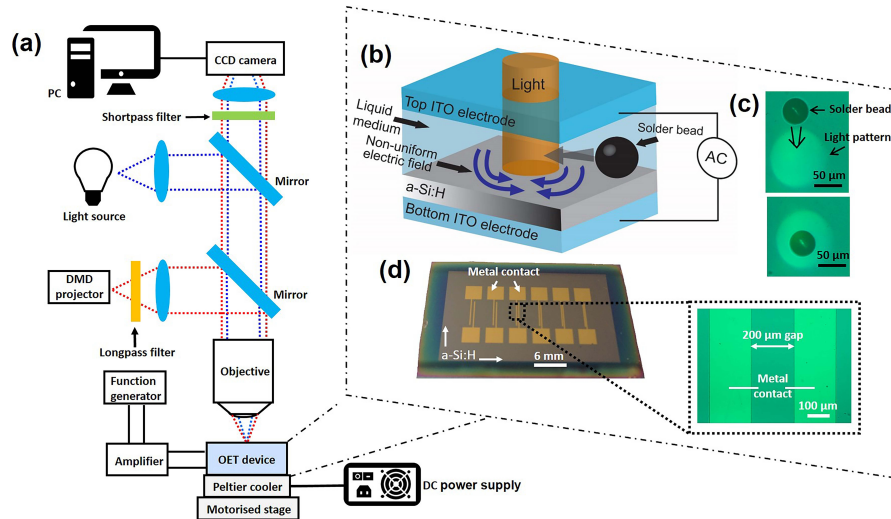


Fig. 1. (a) Schematic experimental setup. (b) 3D schematic of the OET device. (c) Microscope images of a solder microsphere attracted to the illuminated region under positive DEP force. (d) Image of the bottom OET electrode with six pairs of isolated metal contacts with different gaps. Inset: microscope image of the metal contacts with a $200 \mu\text{m}$ gap.

2. Experimental setup and device structure

Figure 1(a) shows the schematic of the optical setup used in the experiment (a separate Appendix section is also provided to show experimental details). As shown in the setup, a digital micro-mirror device (DMD) projector is used to create light patterns which are imaged through the objective of a microscope onto the OET device, which is placed on top of a Peltier cooler. A camera mounted on top of the microscope is used to record experimental images and videos of particles being manipulated in OET for further data analysis. The position of the OET device is controlled by the motorized XY stage while the DMD and camera are kept stationary. A long-pass filter is used to filter out the blue emission from the projector and only the green-red portion of the light emission is projected onto the OET device. A short-pass filter is used in front of the camera to filter out the strong red emission from the projector. This filtering allows the particles to be viewed by bright-field microscopy with just a faint pattern of the intense patterned light from the projector. Figure 1(b) shows a three-dimensional (3D) schematic of the OET device used in this work, which consists of two electrodes, both of them glass slides coated with 600-nm-thick indium tin oxide (ITO). The bottom electrode is also coated with an additional 1- μm -thick hydrogenated amorphous silicon (a-Si:H) photoconductive layer. The two electrodes were attached together by a $150 \mu\text{m}$ thick spacer to form a chamber where inside contains the

sample of liquid medium and the solder beads. In the dark, the impedance of the a-Si:H layer is very high and the applied AC voltage is mainly dropped across this layer. However, when a light pattern is projected on to the a-Si:H layer, the impedance of this layer drops significantly, which makes the voltage drop predominantly across the liquid medium above the illuminated area, thus creating a non-uniform electric field between the dark and illuminated regions in the device chamber. This non-uniform electric field interacts with the samples in the liquid medium producing either attractive (positive DEP force) or repulsive (negative DEP force) depending on their Clausius-Mossotti (CM) factors [7]. Therefore, ‘traps’ can be created to manipulate the positions of samples in the OET device by controlling the positions of projected light patterns. For the solder microspheres used in this work, they were attracted to the illuminated regions under positive DEP force, as shown in Fig. 1(c).

Figure 1(d) shows the images of the bottom electrode of the OET device used in this work. Compared with conventional OET devices, this bottom electrode has six pairs of specifically-designed isolated metal contacts with different gaps (50 μm , 100 μm , 150 μm , 200 μm , 300 μm , 400 μm) on top of the a-Si:H layer. Such design is to demonstrate the use of OET to construct a microscale circuit via the assembly of solder microspheres to form electrical connections between the isolated metal contacts. The bottom OET electrode and top OET electrode were mounted together by a 150 μm thick spacer to form a chamber, where the solution containing solder microspheres were injected via pipette. More information of the structure of the OET device and experimental details can be found in the Appendix.

3. Experiment and discussion

3.1. Parallel assembling, freezing-drying and heating solder microspheres

In this work we assembled the micro solder beads into conductive links by light-patterned DEP in a specifically-designed OET device. The device was mounted onto a Peltier cooler on the microscope stage so that once the desired bead arrangement was achieved it could be cooled down, freezing the liquid buffer. Figures 2(a)-(d) show the process of parallel assembly of 40 μm ($\pm 5 \mu\text{m}$) diameter solder beads in OET to form a straight line to connect two isolated metal contacts. Videos showing more details of the assembling process can be found in the supplementary materials ([Visualization 1](#), [Visualization 2](#)). Shown in Fig. 2(a) is the first step of the assembling process, in which the solder beads were moved to interface with the metal contacts. When a light pattern is used to trap a bead and gradually moves to the metal contact, the bead will follow the light pattern and stop at the edge of metal contact as a strong electrical gradient is formed at the edge of the metal, drawing the beads towards it. However, the metal contacts effectively block the applied electrical fields preventing the beads from being moved further onto them. After manipulating the solder bead to interface with metal contact on each side, more solder beads were precisely manipulated and positioned to fill in the gap to form a straight line, as shown in Figs. 2(b) and 2(c). During the assembling process, multiple light patterns were used to move the beads to fill in the gap and also to fix the solder beads which have already been positioned in place. This parallel manipulation prevents the interactions between the solder beads pushing each other away from their desired positions, allowing the solder beads to gently touch each other. After all the solder beads were assembled, the projector used to produce the light patterns was turned off and the assembled beads would stay in place (see Fig. 2(d)) [20]. It is worth mentioning that the solder beads can be positioned quickly with high positional accuracy under strong DEP force in the OET device (see [Visualization 1](#), [Visualization 2](#)) [20, 21]. Additionally, compared with widely used transfer-printing technology based on using robotic arms and stamps/tips to ‘pick and place’ targeted objects [27–29], OET is capable of performing effective touchless parallel manipulation of objects in the same plane, allowing the solder beads to be precisely assembled next to each other in real time. This makes OET a useful tool to perform the assembly of solder beads or similar metallic micro-objects for potential applications such as device microfabrication

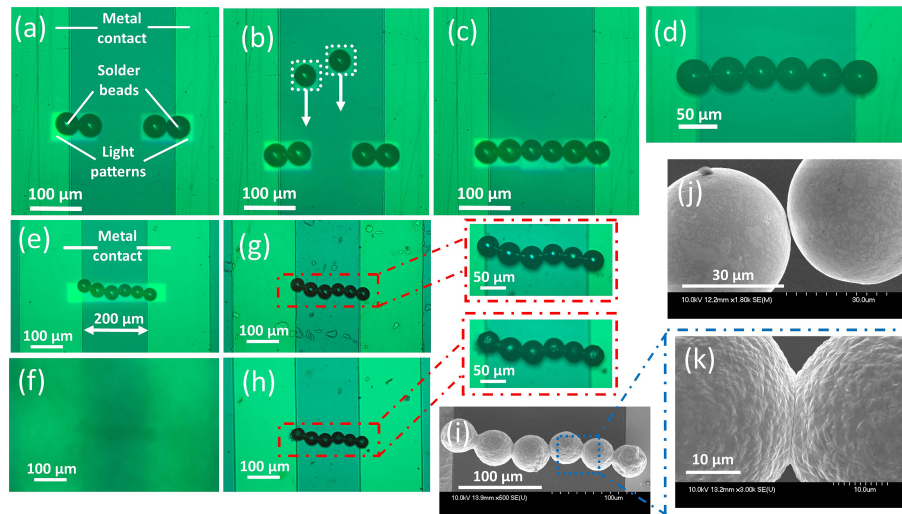


Fig. 2. Parallel assembling, freezing-drying and heating the solder beads. (a) Microscope image of the solder beads positioned at the edge of the metal contacts. (b) Microscope image of parallel assembly of solder beads to fill in the gap and form the straight line. (c) Straight line of solder beads formed by the light patterns. (d) Microscope image of formed straight line of solder beads after turning off the DMD projector. Videos showing the detailed assembling process of solder beads can be found in [Visualization 1](#), [Visualization 2](#). Microscope images of solder beads: (e) after assembling the solder beads, (f) after freezing the solder beads, (g) after sublimating the liquid medium, (h) after heating the solder beads. (i) SEM image of the assembled solder beads after heating. (j) SEM image of two adjacent solder beads before heating. (k) SEM image of two adjacent solder bead after heating.

and precise circuit construction. It is worth mentioning that OET has been demonstrated to be a compatible micromanipulation technology capable of assembling many different nano- and micro-scale objects, ranging from semiconductor nanowires and carbon nanotubes [17, 18], to metallic and dielectric particles on the order of tens of microns [10, 11, 20], to photonic/electronic devices with sizes greater than 100 microns [21, 22]. Additionally, alignment of particles with OET can be made as the assembly is ongoing in a way that would not be possible with either photo or e-beam lithography, giving added flexibility to the fabrication process. Therefore, we believe that OET has a great potential for micro-assembly applications on its own or together with other techniques, such as photolithography and 3D printing, if necessary.

Figures 2(e)-(h) show a complete process of assembling, freeze-drying, and heating the solder beads. This process is not the same process shown in Figs. 2(a)-(d). Experimental results and discussions of freeze-drying and its influence on bead position will be presented later. As shown in Fig. 2(e), the solder beads were firstly assembled into a straight line to connect two isolated metal electrodes with a 200 μm gap. Then, the OET device was frozen by the Peltier cooler to preserve the assembled beads (see Fig. 2(f)). After the liquid medium was removed via freeze-drying (see Fig. 2(g)), the assembled solder beads were heated and melted to connect with each other (see Fig. 2(h)). After the heating process, the morphology of the solder bead changes and the physical connections appear at the interface between adjacent solder beads. To provide more details of the morphology change of the beads, SEM images were taken before and after heating the solder beads. Figure 2(i) shows SEM image of the assembled solder beads between the metal contacts after heating, in which the beads show rough and textured surfaces. This contrasts with the solder beads before heating (see Fig. 2(j)), in which the beads show smooth surfaces. More detailed morphology changes of the solder beads can be found in Fig. 2(k), in which the fused

structure between the adjacent solder beads is formed after the heating process. These SEM images provide clear evidence to show that the heating process melts the solder beads and makes the material on the surface of the bead flow toward the interfaces between the adjacent solder beads, forming the observed fused structure.

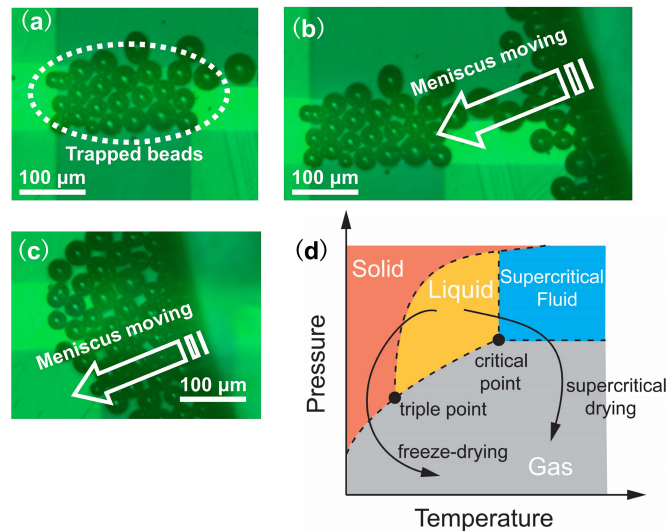


Fig. 3. (a) Trapped solder beads in OET device. (b)&(c) Trapped solder beads were dragged away by meniscus during the process of evaporating the solution. See [Visualization 3](#) for a video showing the detailed process. (d) Phase diagram of supercritical drying which goes beyond the critical point (high pressure/high temperature regime) and the freeze drying which goes below the triple point (low pressure/low temperature regime).

3.2. Freeze-drying

After assembling micro particles into a desired arrangement for many applications, it is necessary to remove the liquid medium. This allows the assembled components to be further processed, used as a device or stored in a stable state. However, as the micromanipulation forces are small compared to the forces needed to overcome the surface tension of the liquid medium during the solution evaporating process, the particles will be moved as the meniscus passes over them thus making the assembled structure difficult to preserve. Figures 3(a)-(c) show the influence of the liquid evaporating process on the assembled structure with meniscus passing over it. A video showing the detailed process can be found in the supplementary materials ([Visualization 3](#)). It is possible to reduce this effect with organic solutions with smaller surface tension coefficients such as Isopropyl alcohol and Methanol to replace the deionized (DI) water solution. However, it is found that even with organic solutions, the assembled structure cannot be preserved well making it necessary to develop another method to remove the liquid medium from the OET device. To address this issue a method based on freeze-drying was developed. Here we freeze the solution and then reduce the surrounding pressure to allow the frozen medium to sublimate directly from the solid phase to the gas phase. This results in no meniscus passing over the particles, hence preserving their arrangement. Similar procedures have been adopted in micro-electro-mechanical system (MEMS) technologies [30]. Here the problem is that MEMS components that are designed to be free from the surface become stuck if processed in a liquid and then dried out by conventional blow drying. Switching the water with methanol before evaporation, sublimation drying with alcohol, and supercritical drying with CO_2 have all been assessed with both sublimation and

supercritical drying producing good results [30]. Shown in Fig. 3(d) is the phase diagram of supercritical drying and freeze-drying, while both cases avoid the direct liquid-gas transition. Supercritical drying requires going from the liquid to the gas phase around the high pressure/high temperature side of the liquid's critical point where the difference between liquid and gas become indistinct. By instead going from the liquid to the solid phase first and then to the gas phase, freeze-drying is easier to implement under a microscope in a typical micromanipulation setting and so this is the process that we developed. To freeze the liquid medium while avoiding moving the OET device, a Peltier cooler was coupled to the bottom of the OET device (see Fig. 1(a)). After the liquid medium was visibly frozen the OET device was put into a freezer (RS Biotech Eclipse 100) and kept at -80°C for 10 minutes ensuring the completion of the freezing process. Then, the OET device was transferred to a freeze dryer (Thermo Heto PowerDry LL3000) to sublimate the frozen medium for 30 minutes. After the frozen medium was sublimated, the top ITO electrode of the OET device was removed to expose the assembled solder beads. During the experiment, it was found that a rapid freezing process can move the positions of the assembled solder beads and break the assembled pattern. Therefore, quantitative measurements were carried out to study the influence of freezing process on the finished structure.

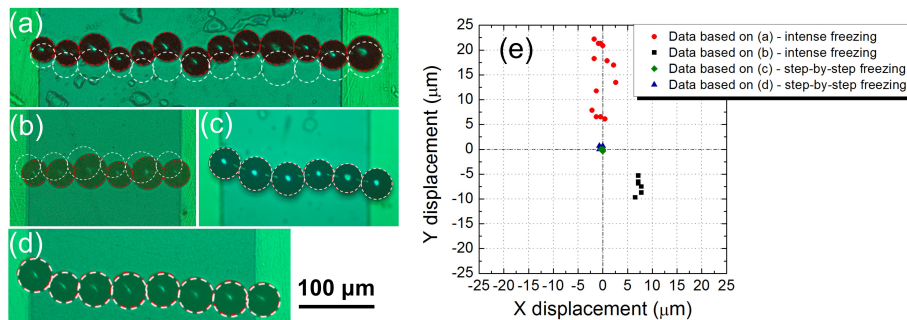


Fig. 4. Experimental results of the solder bead before freezing the solution and after sublimating the frozen medium. (a)-(d) Microscope images of the assembled solder beads before freezing the solution (outlined in white) and after sublimating the frozen medium (outlined in red) under different freezing conditions, in which rapid freezing was used for (a) and (b); step-by-step freezing was used for (c) and (d). Shown in (e) is the distribution of moving distances (in X-axis and Y-axis) of solder beads before freezing the solution and after sublimating the frozen medium. The moving distances are calculated based on the microscope images shown in (a)-(d).

Shown in Fig. 4 are the results of the freezing step with the solder bead before freezing the solution (outlined in white) and after sublimating the frozen medium (outlined in red) under different freezing conditions. Figures 4(a) and 4(b) show the experimental results based on a quick freezing process, in which the Peltier cooler was driven continuously at 3 A for 10 minutes to freeze the liquid medium in the OET device. The temperature profile produced is shown in Fig. 5(a) with the device reaching a temperature of -10°C in 320 seconds. As shown, the beads moved away from where they are placed under this rapid freezing process. Figures 4(c) and 4(d) show the experimental results under an optimized step-by-step freezing process, in which the Peltier cooler was driven at 1 A for 2 minutes, 1.5 A for 2 minutes, 2 A for 2 minutes, 2.5 A for 3 minutes and 3 A for 5 minutes (see Fig. 5(b)). In this case, the freezing process is optimized to preserve the assembled solder beads by gradually increasing the input current of the Peltier cooler so that cooling to -10°C took 540 seconds. Under this step-by-step freezing process, the assembled solder beads can remain where they are placed after the sublimation process, as shown in Figs. 4(c) and 4(d). The distances moved by the beads are plotted for two different freezing processes and shown in Fig. 4(e). It can be seen that rapid freezing can move the beads by over

20 microns whilst slowly freezing can keep the bead displacement to less than one micron. These results suggest that the freeze-drying method containing step-by-step freezing and sublimation can preserve the assembled microstructures of solder beads whilst removing the liquid solution. Interestingly, under the rapid freezing process, the assembled solder beads didn't move randomly from where they are placed; instead, they moved in a similar direction. This suggests that the movement is due to the crystallization process of the liquid medium, which starts at one side of the device and generates a force to move the beads at the interface between the solid phase (ice) and the liquid phase. For a free liquid droplet on a cold plate, the geometry of the freezing front results in a tip being formed on the frozen droplet [31]. However here we have two plates which the water freezes between producing a predominantly horizontal movement of the freezing front. The crystallization process tends to follow a specific direction pushing the beads along with it in horizontal plane (see Fig. 6(a)). In the step-by-step slow freezing process, the OET device may be cooled more uniformly allowing the crystallization process of the liquid to start at the bottom of the OET device and proceed vertically through the device inducing less horizontal freezing motion (see Fig. 6(b)). These results suggest the advantage of using freeze-drying to preserve fragile structures assembled by OET. More details of using freeze-drying to dry out MEMS structures and the advantage of reduced mechanical and thermal stresses were well described previously [30].

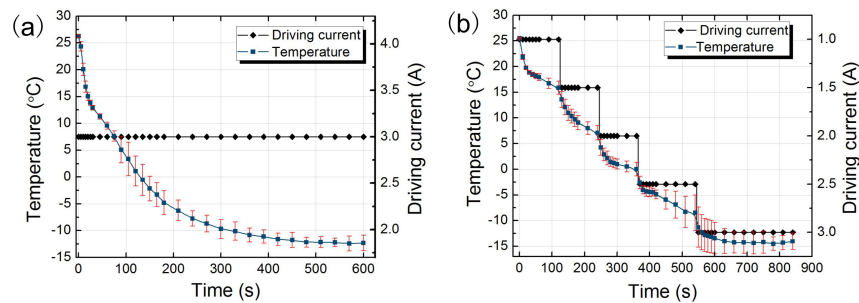


Fig. 5. (a) Temperature profile of OET device with the Peltier cooler being driven at 3A for 10 minutes (quick freezing). (b) Temperature profile of OET device with the Peltier cooler being driven at 1 A for 2 minutes, 1.5 A for 2 minutes, 2 A for 2 minutes, 2.5 A for 3 minutes and 3 A for 5 minutes (step-by-step freezing).

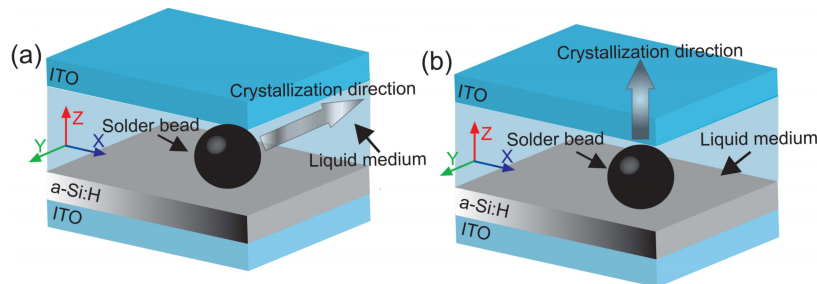


Fig. 6. 3D schematic of the movement of a solder bead under different freezing conditions. (a) Schematic of a solder bead moved horizontally under the rapid freezing. (b) Schematic of a solder bead stabilized horizontally under the step-by-step freezing process.

3.3. I-V measurement

After assembling the solder beads and subsequently removing the liquid medium via freeze-drying, the OET device was placed on top of a hotplate (Cole-Parmer StableTemp) at 185 °C for five minutes to heat and melt the assembled solder beads (melting point 178 °C - 180 °C). The experimental results of assembling, freezing-drying and heating solder beads have been shown in Figs. 2(e)-(k). The current-voltage (I-V) characteristics of the isolated metal contacts connected by the solder beads were measured by a semiconductor device analyzer (Keysight B1500A) using a probe station (Casca-deMicrotech MPS150). As shown in Fig. 7(a), the resistances between the isolated metal contacts before and after assembling the solder beads (without heating) were measured to be around $10^8 \Omega$ and $10^7 \Omega$, respectively. The drop of the resistance is due to the assembled solder beads, however, it is still very large. Figure 7(b) shows the I-V characteristic of the circuit after heating the assembled solder beads and the resistance was measured to be 11.6 Ω . In this case, the assembled solder beads bridge an effective conductive path between the isolated metal contacts, inducing a significant drop of the resistance between the metal contacts. The SEM images show that the heating process melted the material from the surface of the solder beads and formed a fused structure between the adjacent solder beads, significantly reducing the interface resistance between them. The SEM images also show that the adjacent beads are fused together with a contact area over ten microns across. If the lithographically patterned contacts were connected by a single bar of solder tens microns in diameter over the 200 μm gap it is expected that the resistance of this bridge would be less than 1 Ω according to the calculation shown in the Appendix. The fact that the bridge produced is more resistive than this suggests that the measured resistances are still dominated by the interfaces between beads and between the beads and the metal contacts even after the melting stage. Therefore, relevant work is currently on going to reduce the interface resistance by optimizing the heating process such as adjusting the temperature, time and sample's ambient heating environment to create more conductive interfaces between the beads. Since the solder beads have a great potential to be used for creating electrical connections, our future work in this area will focus on using OET to assemble solder beads together with photonic and electronic components to make functional devices. A proof-of-concept demonstration of using OET to assemble solder beads and a micro-sized light-emitting diode (micro-LED) [32, 33] can be found in the Appendix.

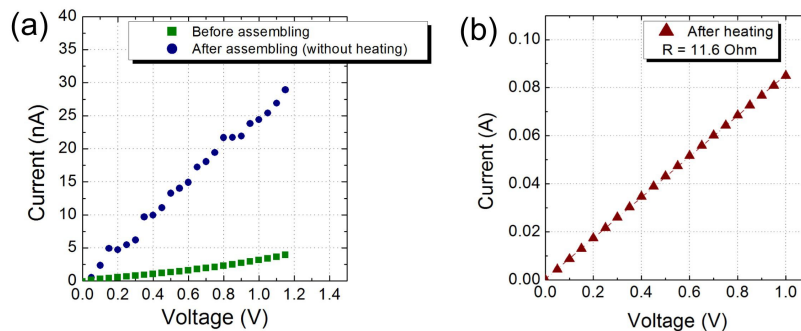


Fig. 7. I-V characteristics. (a) I-V characteristics of the isolated metal contacts before and after assembling the solder beads (without heating). (b) I-V characteristic of the isolated metal contacts after heating the assembled solder beads.

4. Conclusion

In summary, this work demonstrates how freezing and subsequent sublimation can be used to preserve the arrangement of micro-particles assembled through optical micromanipulation

techniques in a liquid environment. We have shown that by using a slow, step-by-step, freezing process micro solder beads can be preserved in a desired arrangement to within one micrometer of their initial positions whereas quickly freezing the solution can cause them to move by tens of microns. We further show that this level of control is sufficient to allow the subsequent fusing together of the solder beads by heating and melting them and that this fused connection has a relatively low resistance. Additionally, the OET device is capable of performing parallel manipulation of solder beads in the same plane, allowing the beads to be precisely assembled and interfaced with each other or other small electronic components which then is an enabling step towards manufacturing electrical circuits using OET rather than pick and place technologies. The freezing and subsequent freeze-drying process developed here however will be more generally applicable to other tweezing modalities such as optical, acoustic or magnetic tweezing allowing the preservation of patterned micro-particles for many applications.

5. Appendix

5.1. Sample preparation

The solder beads used in this work are commercially-available $\text{Sn}_{62}\text{Pb}_{36}\text{Ag}_2$ microspheres (Industrie des Poudres Sphériques, France), which are in powder formats as provided from the company. To make the sample for the experiment, the beads were put into a solution, consisting of deionized water with 0.05% volume ratio of non-ionic surfactant TWEEN 20 (SIGMA P9416). Since the solder beads tend to 'clump together' in random complexes and stick onto the surface of pipette, adding TWEEN 20 in the solution can minimize the clumps and help transfer the beads into the OET device. The conductivity of the solution was measured to be 2 mS m^{-1} after adding the TWEEN 20. To carry out the experiment, the solution containing the metallic microspheres was injected into the OET device at a volume of $10 \mu\text{L}$ each time using a pipette and the device was biased with a 15 kHz 25 V peak-to-peak AC signal.

5.2. Device fabrication

The OET device used in this work consists of a top electrode and a bottom electrode. The top electrode is made from a standard microscope glass slide ($2.5 \text{ cm} \times 7.5 \text{ cm} \times 1 \text{ mm}$) coated on one side with 600 nm thick ITO by magnetron sputtering (Diamond Coating Ltd, UK) (see Figs 8(a) and 8(b)). To make the top electrode, the ITO-coated glass slide was cut to small pieces with sizes around $2.5 \text{ cm} \times 1.5 \text{ cm}$ using a diamond scribe. An electrical wire was bonded to the small piece of ITO-coated glass slide using a conductive silver paint (Agar Scientific, Acheson Silver DAG 1415M) and an epoxy resin (Mxbon Waterproof Epoxy-E41A). Image of the top electrode can be found in Fig. 9(a).

Shown in Fig. 8 is the fabrication flow of the bottom electrode. Compared with the top electrode, an extra photoconductive layer made of a-Si:H was deposited on top of the ITO layer at a thickness of $1 \mu\text{m}$ by plasma-enhanced chemical vapour deposition (PECVD) (Oxford Instruments PECVD 80+) (see Fig. 8(c)). On top of the a-Si:H layer, a SiO_2 insulation layer with a thickness of 350 nm was also deposited by PECVD (Oxford Instruments PECVD 80+) (see Fig. 8(d)). Then, a standard photolithography process was used to define photoresist patterns on top of the SiO_2 layer (see Figs. 8(e) and 8(f)). After the photoresist patterns were formed, reactive ion etching (RIE) (Oxford Instruments RIE80+) was used to remove specific parts in the SiO_2 layer and expose the a-Si:H layer (see Fig. 8(g)). Then, acetone (CH_3COCH_3) was used to remove the photoresist patterns. The following step was to use standard photolithography to redefine the photoresist patterns (see Figs. 8(h) and 8(i)). After this step, the exposed a-Si:H layer was covered by photoresist while there is no photoresist on top of the SiO_2 layer (see Fig. 8(i)). After depositing a thin metal layer consisting of Ni/Au (10 nm/ 90 nm) using an electron beam evaporator (Plassys MEB 550S) (see Fig. 8(j)), a metal lift-off process was used to remove the

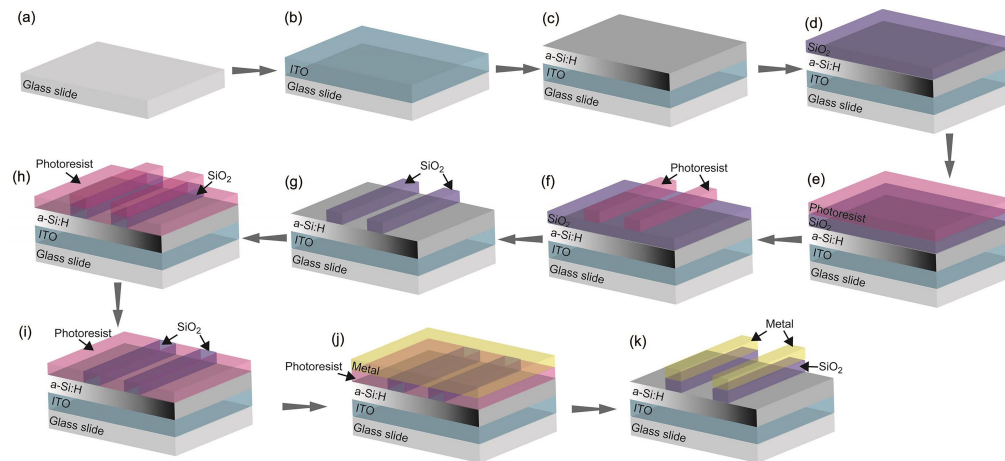


Fig. 8. (a)-(k) Step-by-step fabrication flow of the bottom OET electrode.

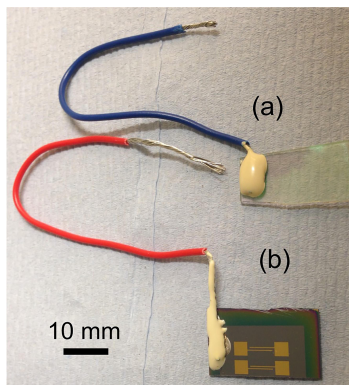


Fig. 9. Image of the OET device. (a) Image of the top OET electrode used in this work. (b) Image of the bottom OET electrode used in this work.

metal deposited on top of the photoresist. Therefore, specifically-designed metal contacts can be fabricated on top of the a-Si:H layer with SiO₂ insulation layer sandwiched in between (see Fig. 8(k)). To make the bottom electrode, the ITO-coated glass slide with a-Si:H layer and metal contacts was also cut to small pieces with sizes around 2.5 cm × 1.5 cm. Then, a scratch knife was used to remove the a-Si:H at the edge to expose the conductive ITO layer, where an electrical wire was mounted using silver paint and epoxy as for the top electrode. An image of the bottom electrode can be found in Fig. 9(b). After the top and bottom electrodes were fabricated, they were attached together by a 150 μm thick spacer to form a chamber, where the liquid medium containing the solder beads was injected via a pipette. This attached electrode pair formed the OET device used in this work.

5.3. Used equipment

The equipment used for the experimental setup (see Fig. 2) includes a DMD projector (Dell 1510X), a microscope (Olympus BX51 microscope, with motorized Prior Scan111 stage), a Peltier cooler (ETH-127-14-15-RS), an amplifier (Thurlby Thandor Instrument WA31 amplifier), a function generator (TG5011 LX1 function generator), a long-pass filter (Thorlabs FD1R) and a short-pass filter (Thorlabs FES0550). An infrared camera (FLIR E60bx) was also used to

measure the temperature profiles of the OET device cooled by the Peltier.

5.4. Resistance calculation

A simplified model of solder bar (cylinder) was used to calculate the resistance of the bridge formed by the solder beads. For a single bar of solder with $10\ \mu\text{m}$ in diameter over the $200\ \mu\text{m}$ gap, it is expected that the resistance of this bar would be:

$$R = \rho \cdot \frac{\text{Length}}{\text{Area}} = \frac{\rho \cdot l}{\pi \cdot r^2} \quad (1)$$

For the solder bead used in this work, the electrical resistivity (ρ) is $0.145\ \Omega \cdot \mu\text{m}$; L is $200\ \mu\text{m}$; r is $5\ \mu\text{m}$. Therefore, the resistance of the bar is calculated to be $0.4\ \Omega$.

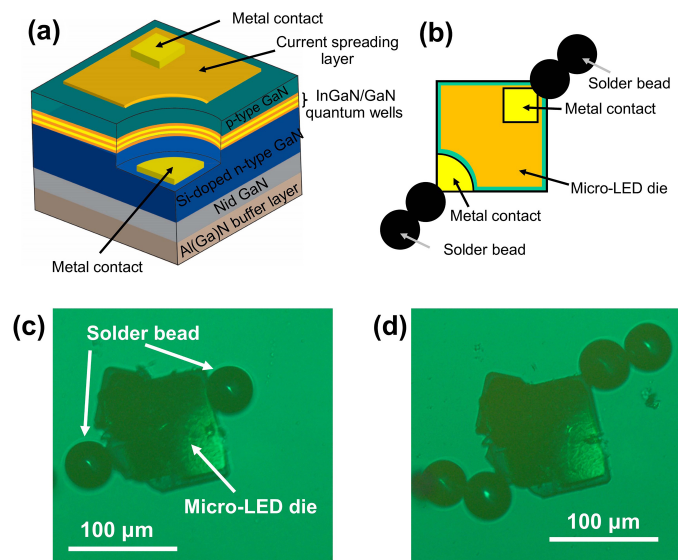


Fig. 10. (a) Schematic of the micro-LED device. (b) Schematic layout of connecting solder beads to the metal contacts of a micro-LED device. (c) & (d) Microscope images of solder beads assembled by OET to connect with the metal contacts at the corners of the micro-LED device.

5.5. Assembling of the solder beads with the photonic device

Figure 10 shows the micro-assembly of solder beads to connect with the metal contacts of a micro-sized light-emitting diode (micro-LED) device using OET. The detailed device structure and fabrication procedures can be found in previously reported work [32, 33].

Funding

Engineering and Physical Sciences Research Council (EPSRC) (EP/L022257/1, EP/L00044X/1).

Acknowledgements

The authors thank the staff of James Watt Nanofabrication Centre (JWNC, Glasgow, UK) for their help on device fabrication.